Response of glassy liquids to thermal gradients

Vinay Vaibhav,[1,2] Jürgen Horbach,[3] and Pinaki Chaudhuri[1,2]
[1]*The Institute of Mathematical Sciences, CIT Campus, Taramani, Chennai 600113, India*
[2]*Homi Bhabha National Institute, Anushaktinagar, Mumbai 400094, India*
[3]*Institut für Theoretische Physik II, Heinrich-Heine-Universität Düsseldorf, Universitätsstraße 1, 40225 Düsseldorf, Germany*

(Received 31 December 2018; revised manuscript received 7 January 2020; accepted 8 January 2020; published 14 February 2020)

The Soret effect, i.e., the flow of matter caused by a temperature gradient, is studied in a glass-forming binary Lennard-Jones (LJ) mixture, using nonequilibrium molecular dynamics computer simulation. The transport processes associated with this effect are thermal diffusion and interdiffusion. While interdiffusion processes exhibit a drastic slowing down when approaching the glass transition, thermal diffusion appears to be a fast process even in the glass. We show that the Soret effect becomes more pronounced in the vicinity of the glass transition, due to the decoupling between thermal diffusion and interdiffusion as well as the chemical ordering in the considered LJ mixture. This is reflected in the occurrence of large concentration gradients, nonlinear concentration profiles, and long-lived nonstationary structures.

DOI: 10.1103/PhysRevE.101.022605

I. INTRODUCTION

Many glass-forming liquids are intrinsically polydisperse or multicomponent in their constituent properties [1], via which crystallization is kinetically suppressed and thus glasses are formed. Multicomponent glasses, in various form, are ubiquitous in diverse applications or natural phenomena and in many such cases the nonequilibrium response of such systems to external stimuli, e.g., heat or mechanical load, is of significance. However, from a microscopic perspective, the response to externally imposed temperature gradients, especially even of binary glass-forming liquids, is not well understood. Here, we focus on this issue using nonequilibrium molecular dynamics (MD) simulations.

When a temperature gradient is applied to any mixture, there is a resultant flux of matter. This is known as the Ludwig-Soret effect [2–4], which has been extensively studied [5–11] in fluid mixtures under "normal conditions," i.e., far away from the glass transition. In the linear response regime, for a binary mixture with an asymmetry, e.g., in size, charge, mass, or interaction energy, this effect is characterized by the Soret coefficient, defined as $S_T = D_T/D_{AB}$ with D_{AB} the interdiffusion coefficient and D_T the thermal diffusion coefficient. While D_T is a measure of the cross-correlations between thermal and mass fluxes, D_{AB} is associated with the mass transport induced by concentration gradients. Thus, S_T measures the relative strength of the latter processes.

For glassy materials, inhomogeneous thermal conditions are encountered under diverse circumstances, e.g., during the formation of the glass from the supercooled melt via cooling [12–15], via densification [16], or in cases where the material is heated nonuniformly [17–19]. During the glass formation, there is a fundamental difference between the transport of heat and processes such as interdiffusion which are associated with the mass transport. Structural relaxation becomes increasingly slow as the glass transition is approached, and, as a consequence, a drastic slowing down and eventually a dynamical arrest of the interdiffusive transport takes place. The heat flux, however, remains a fast process in the supercooled liquid and even in the glass state [20–23].

Our objective is to investigate the coupling between thermal diffusion and interdiffusion processes, as the ambient temperatures are varied from the supercooled to the glassy regime. In the vicinity of the glass transition, one may expect a strong nonlinear coupling of the two transport processes as well as long-lived nonstationary structures, at least in regions where the local temperature is below the glass transition temperature.

Using extensive MD simulations, we investigate the response of a model glass-forming liquid to an applied thermal gradient. We show that with decreasing temperature the concentration gradients increase and the nonlinear response sets in at smaller thermal gradients. However, in the glass state, the prohibitively slow dynamics suppresses the onset of such concentration inhomogeneities in response to the thermal gradient. Here, local melting in zones above the glass transition temperature leads to various anomalies, including history-dependent responses. Below, we show that our observations are due to the negative mixing enthalpy of the considered glass-forming mixture as well as the decoupling in the dynamical behavior of the constituent species.

The paper is organized in the following way. In Sec. II, we describe the details of the model glass former that is used for the MD simulations, as well as the numerical method used for probing the nonequilibrium response of the system. In Sec. III, we discuss the findings of our paper, and then we provide a concluding discussion in Sec. IV.

II. MODEL AND METHOD

For our paper, we consider the well-studied glass-forming Kob-Andersen 80:20 binary AB Lennard-Jones (LJ) mixture, originally proposed to model amorphous $Ni_{80}P_{20}$ [24]. The

interaction between two constituent particles has the form

$$V_{\alpha\beta}(r) = u_{\alpha\beta}(r) - u_{\alpha\beta}(R_c) - (r - R_c)\left.\frac{du_{\alpha\beta}}{dr}\right|_{r=R_c},$$

$$u_{\alpha\beta}(r) = 4\epsilon_{\alpha\beta}[(\sigma_{\alpha\beta}/r)^{12} - (\sigma_{\alpha\beta}/r)^{6}], \quad (1)$$

for $r < R_c$, with $\alpha, \beta = \mathrm{A}, \mathrm{B}$. Following Ref. [24], we have chosen $\epsilon_{\mathrm{AA}} = 1.0$, $\epsilon_{\mathrm{AB}} = 1.5\epsilon_{\mathrm{AA}}$, and $\epsilon_{\mathrm{BB}} = 0.5\epsilon_{\mathrm{AA}}$ for the parameters with units of energy and $\sigma_{\mathrm{AA}} = 1.0$, $\sigma_{\mathrm{AB}} = 0.8\sigma_{\mathrm{AA}}$, and $\sigma_{\mathrm{BB}} = 0.88\sigma_{\mathrm{AA}}$ for those with units of length. The range of the interactions is set to $R_c = 2.5\sigma_{\mathrm{AA}}$. All particles have the same mass $m = 1$. All measured quantities are expressed in LJ units, whereby lengths and energies are expressed in units of σ_{AA} and $\varepsilon_{\mathrm{AA}}$, respectively. The unit of time is $\sqrt{m\sigma_{\mathrm{AA}}^2/\varepsilon_{\mathrm{AA}}}$.

For this model, the mode-coupling temperature, below which equilibrium dynamics is difficult to observe, occurs around $T_{\mathrm{MCT}} = 0.435$ and the glass transition is estimated at $T_{\mathrm{VFT}} \approx 0.3$. Note that the majority A species and the minority B species have a size asymmetry, $\sigma_{\mathrm{AA}}/\sigma_{\mathrm{BB}} \approx 1.14$, and the choice of the energy parameters in the LJ model, $\varepsilon_{\mathrm{AB}}/\varepsilon_{\mathrm{AA}} = 1.5$ and $\varepsilon_{\mathrm{AB}}/\varepsilon_{\mathrm{BB}} = 3.0$, provides a negative mixing enthalpy and a strong stability against fluid-fluid demixing [25–27].

In our paper, we consider a system of $N = 22\,500$ particles in a rectangular box of dimension $L_x = L_y = 14.12$ and $L_z = 94.10$, with periodic boundary conditions. The MD simulations are carried out by numerically integrating the equations of motion of the N particles via the velocity Verlet algorithm, with a time step of $\delta t = 0.005$, using LAMMPS [28].

Both in the equilibrium and nonequilibrium simulations, respective global and local temperatures are maintained via Langevin thermostat, using a dissipation timescale of $\tau_d = 0.5$. At temperatures where this model system behaves as an equilibrium liquid, we first equilibrate it by coupling it to the thermostat to maintain the desired temperature T_m. To study the response to a thermal gradient, we locally thermostat a region of width $L_z/10$ in the middle at lower temperature T_{c} [marked "Cold" in the schematic diagram, Fig. 1(a)] and another two regions of width $L_z/20$ at the two extreme ends at higher temperature T_{h} [marked "Hot" in Fig. 1(a)] [5]. T_{h} and T_{c} are chosen symmetrically about the mean temperature T_m. The intermediate regions adapt to these thermal baths, and we thereby study the response to the applied gradient.

All measurements are averaged over 30–65 independent trajectories, by separately quenching high-temperature liquid ($T = 3.0$) states to different target temperatures (T_m) in the supercooled regime, followed by a sufficiently long run to reach equilibrium, in respective trajectories, at that temperature. The well-equilibrated configurations are prepared for the temperatures 1.0, 0.9, 0.8, 0.7, 0.6, 0.55, and 0.5, and their number varies, e.g., 65 for $T_m = 0.5$ and 30 for $T_m = 1.0$. Similarly, around 65 independent glassy states at $T_m = 0.2$ are prepared by quenching high-temperature liquid states to this temperature, and then each configuration is aged for a period of $t_{\mathrm{age}} = 10^4$.

In the nonequilibrium simulations, after imposing the temperature gradient to the prepared states, spatial profiles of different quantities like heat flux, concentration, density, etc., are measured using 80 bins along L_z. In the supercooled regime, measurements are done when the system reaches the steady state (as described below), while measurements for glassy states are done during the transient regime, since steady state in terms of spatial variation of concentration is not reached. The total length of runs, after switching on the gradient, has been done for 6×10^8 time steps for lower temperatures like $T_m = 0.5$ and 3×10^8 time steps for higher temperatures like $T_m = 1.0$. In the case of $T_m = 0.2$, the glass samples have been exposed to a thermal gradient for 10^8 time steps.

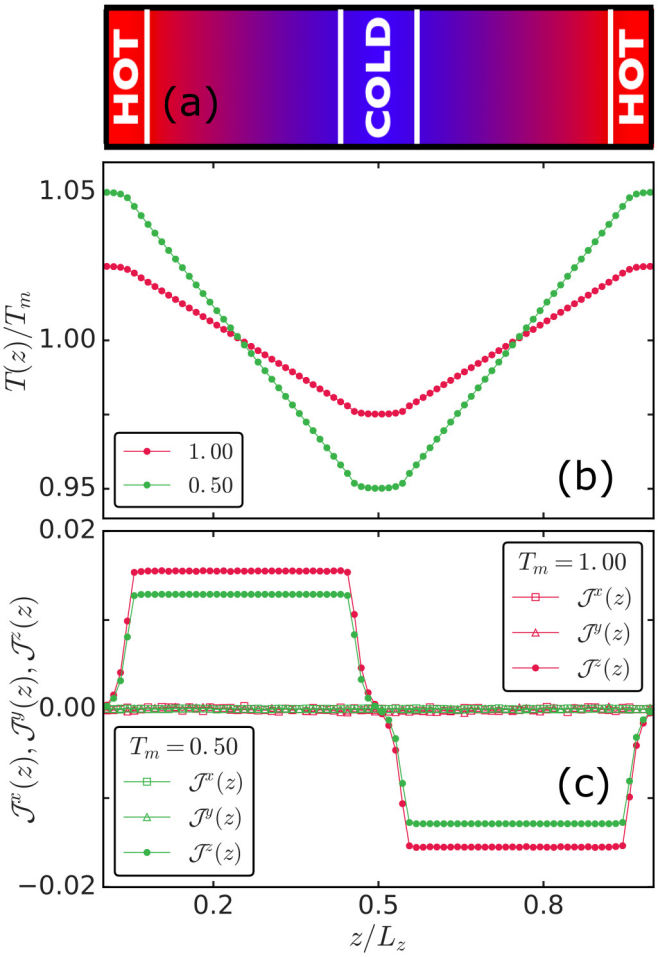

FIG. 1. (a) Schematic of the simulation setup. (b) Typical spatial profile of temperature along z direction, shown for $T_m = 0.5, 1.0$. (c) Corresponding spatial profiles of the heat current along the x, y, z direction.

III. RESULTS

A. Response in the supercooled regime

We first consider the case where the mean temperature T_m resides at temperatures in the supercooled liquid regime. Figure 1(b) shows examples of the linear temperature profiles that are set up, keeping $T_{\mathrm{h}} = T_m + 0.5\Delta T$ and $T_{\mathrm{c}} = T_m - 0.5\Delta T$ between the hot and cold ends, respectively. Correspondingly, there is a finite heat current, $J^z(z)$, that develops in the z direction, and no currents in the orthogonal directions, as is shown in Fig. 1(c). The measurement of heat current density in a bin is done via the following expression: $J^\alpha = \sum_l J_l^\alpha = \frac{1}{V}\sum_l [\sum_{\beta\in\{x,y,z\}}(e_l\delta_{\alpha\beta} - S_l^{\alpha\beta})v_l^\beta]$, where J^α is one

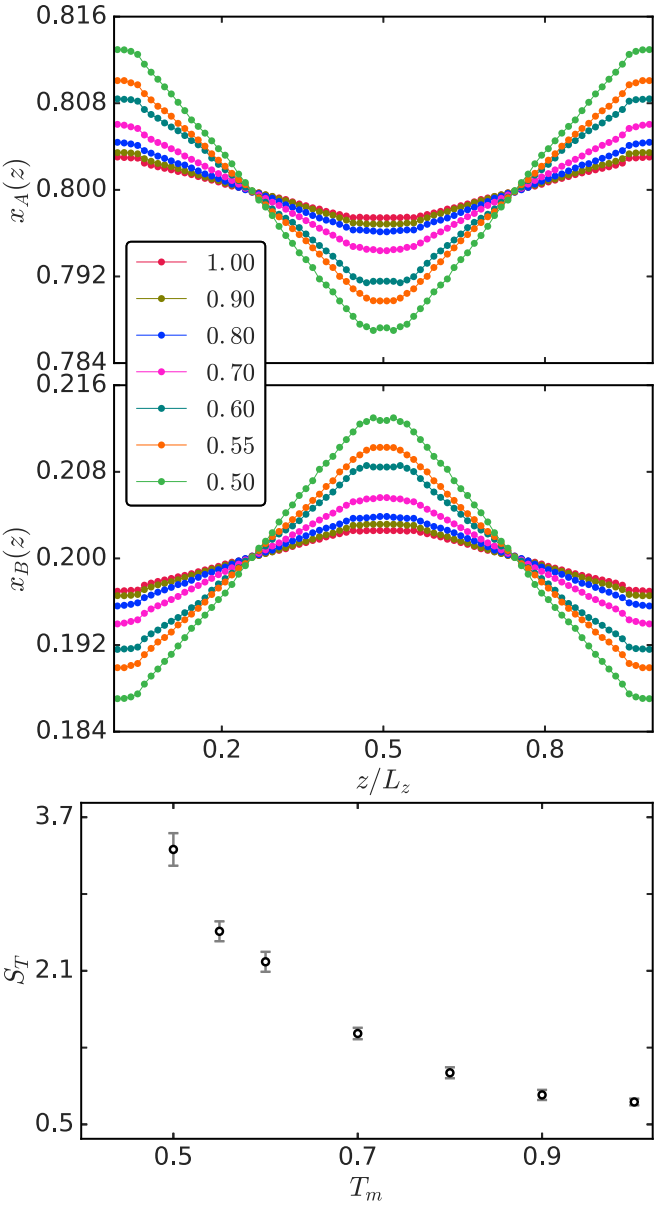

FIG. 2. Top: Spatial concentration profiles of A and B particles, $x_A(z)$ and $x_B(z)$, respectively, for $T_m = 1.00, 0.90, 0.80, 0.70, 0.60, 0.55, 0.50$. Bottom: Variation of corresponding Soret coefficient S_T (absolute value) with T_m.

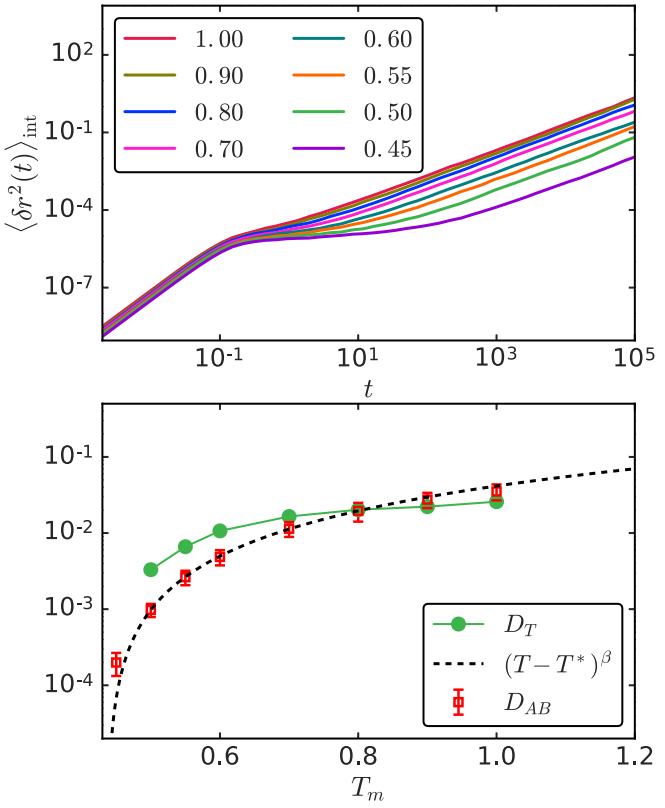

FIG. 3. Top: MSD of the center of mass of A population, $\langle \delta r^2(t) \rangle_{\rm int}$, for different temperatures (as indicated) using equilibrium simulations. Bottom: Corresponding temperature variation of interdiffusion coefficient D_{AB} (shown with red squares), which behaves as $\approx (T - T^*)^\beta$ with $T^* = 0.427$ and $\beta = 1.8$ (shown with dashed line). Also shown is the estimate of thermal diffusivity D_T (shown with green circles), using the relationship $D_T = S_T D_{AB}$.

of the components of the heat current density, l is summed over the number of particles in the bin with volume V, and e_l, v_l^β, and $S_l^{\alpha\beta}$ are the total energy (here, the sum of kinetic and potential energy), component of the velocity, and component of the stress tensor associated with the lth particle in the bin, respectively.

As expected in the steady state, the heat current constantly flows while the mass flux stops and stationary concentration profiles develop; we show these profiles, viz., $x_A(z)$ and $x_B(z)$, respectively, for A and B particles in Fig. 2 (top panel) [29]. The concentration of A species is defined as $x_A(z) = \frac{\rho_A(z)}{\rho(z)}$, ρ and ρ_A being, respectively, the total number density and the density of A species; the concentration of B species is similarly defined. We observe that the concentration of the majority species is higher near the hot end. In steady state, the absolute value of the Soret coefficient has the form $S_T = |-\frac{1}{x_A(1-x_A)}(\frac{\partial x_A}{\partial z})(\frac{\partial T}{\partial z})^{-1}|$ [2,6]. Using this definition, we have computed S_T by doing a straight line fit, locally, to the concentration and temperature profiles, $T(z)$ and $x_A(z)$, respectively, to obtain the local gradients $\frac{\partial x_A}{\partial z}$ and $\frac{\partial T}{\partial z}$. For $x_A(z)$, the fit is done around $x_A = 0.8$ across data points from 20 bins and for $T(z)$, near T_m. We measure the Soret coefficient for the different temperatures, as shown in Fig. 2 (bottom panel), and we observe that its magnitude increases with decreasing temperature. Note that, in our case, the sign of the coefficient is negative for A species, and consequently positive for the B species.

From the temperature dependence of the Soret coefficient, $S_T = D_T/D_{AB}$, we can infer that the thermal diffusivity becomes more dominant ($S_T > 1$) as we approach the glassy regime. Using equilibrium simulations, it is possible to measure the interdiffusion coefficient D_{AB} by tracking the center of mass trajectory of the A species, $\mathbf{R}_A(t) = \frac{1}{N_A}\sum_{j=1}^{N_A} \mathbf{r}_j^A(t)$, and computing the corresponding mean squared displacement, $\langle \delta r^2(t) \rangle_{\rm int} = \langle [\mathbf{R}_A(t) - \mathbf{R}_A(0)]^2 \rangle$, the data for which are shown in the top panel of Fig. 3 for the range of temperatures explored. The interdiffusion coefficient can then be computed

[30] via the "Einstein relation":

$$D_{AB} = \lim_{t\to\infty}\left[1+\frac{x_A}{x_B}\right]^2 \Phi N x_A x_B \frac{\langle \delta r^2(t)\rangle_{\rm int}}{6t},$$

where Φ is the thermodynamic factor, defined as $\Phi = x_A x_B/S_{\rm cc}(q=0)$, $S_{\rm cc}(q)$ being the concentration-concentration structure factor, computed using the partial structural factors $S_{\rm AA}(q)$, $S_{\rm BB}(q)$, and $S_{\rm AB}(q)$ via the expression $S_{\rm cc}(q) = (1-x_A)^2 S_{\rm AA}(q) + x_A^2 S_{\rm BB}(q) - 2x_A(1-x_A)S_{\rm AB}(q)$. In the limit of $q\to\infty$, $S_{\rm cc}(q)\to x_A(1-x_A)$. For the Kob-Andersen binary LJ mixture, Φ does not vary much within the temperature regime of our interest, and is $\approx$2.55.

The temperature dependence of the measured D_{AB} is shown in Fig. 3 (bottom panel) and we demonstrate that the data can be fitted by $D_{AB}\sim (T-T^*)^\beta$, with $T^*=0.427$ and the effective exponent $\beta=1.8$. Thus, in the vicinity of $T_{\rm MCT}$ there is a drastic slowing down of this process and D_{AB} would eventually vanish below the glass transition ($\approx T_{\rm VFT}$). So we can infer from the behavior of the obtained Soret coefficient that D_T, which characterizes the cross-correlation between thermal and mass flux, exhibits a slower decrease than the interdiffusive process, near $T_{\rm MCT}$ as we show in the bottom panel of Fig. 3. However, it also couples to the slow structural relaxation and thus one expects that D_T vanishes below the glass transition temperature. In contrast, even when the supercooled liquid transforms to a glass, the thermal flux and thus the thermal conductivity is finite and decreases continuously [20,21].

The spatial variation in concentration is associated with a variation of the density of each species, as shown in Fig. 4 (middle) and Fig. 4 (bottom) in terms of normalized density profiles of each species, $\tilde\rho_A(z)\equiv\rho_A(z)/\bar\rho_A$ and $\tilde\rho_B(z)\equiv\rho_B(z)/\bar\rho_B$, respectively, with $\bar\rho_A$ and $\bar\rho_B$ the total densities of A and B particles. For both species, the local density is higher at regions where the temperature is lower, and similar is the case with the overall density [see Fig. 4 (top)] which is in agreement with previous observations for a one-component fluid [31]. However, there is also a difference in the response of the two species, such that the enhanced migration of the minority B species to the cold region results in the minimization of the system's total energy and the enhancement of chemical order [32]. This is evidenced in Fig. 5: the emergent concentration profile is such that local equilibrium is satisfied, i.e., for the obtained combination of local x_A and $T(z)$, the local energy measured from nonequilibrium simulations matches with the equilibrium value. The concentration gradient increases when T_m approaches $T_{\rm MCT}$, while maintaining local equilibrium, as demonstrated via the comparative behavior for $T_m=0.6$ and 0.7 in Fig. 5, with the decrease in local temperature leading to lower local energies and a wider range of x_A, via an increased affinity between the A and B species. This is manifested in the increasing density variation, locally, of the minority B species, with decreasing T_m [Fig. 4 (bottom)], while the spatial variation of A species almost remains the same [Fig. 4 (middle)].

We note here that the timescales for the migration of particles over large length scales leading to the emergence of the steady-state density profiles, and thereby the concentration profiles, strongly increase, as local temperatures approach the glassy regime. Thus, for all temperatures in the vicinity of $T_{\rm MCT}$, steady-state conditions for the concentration profiles become difficult to attain, which we discuss below. This slowness contrasts the fast onset of the steady thermal current, which results in anomalies, as further elucidated later.

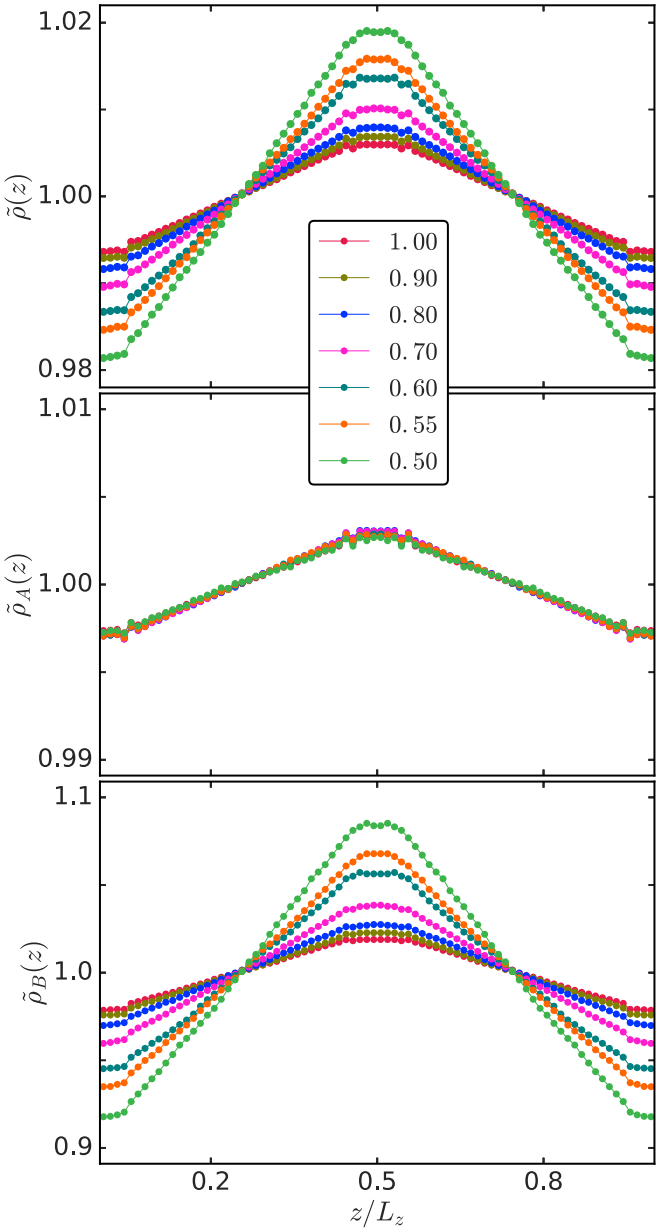

FIG. 4. For different values of T_m (as marked), normalized density profiles (defined in text) for all particles (top) of A species (middle) and B species (bottom).

B. Supercooled liquid: Nonlinear response

We now explore the question of how the concentration profiles change when the applied thermal gradient, dT/dz, is varied. In Figs. 6(a)–6(e), we illustrate the case for $T_m=0.7$. For all considered values of dT/dz, a linear temperature profile [Fig. 6(a)] and a linear dependence of the corresponding heat current on dT/dz [see Fig. 7 (top)] imply that the thermal response is within the linear regime.

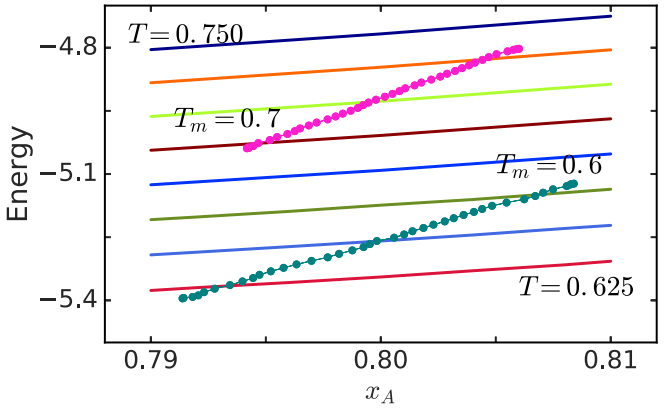

FIG. 5. Local energy vs local concentration, shown for $T_m = 0.6$ (cyan) and 0.7 (pink), superposed on corresponding equilibrium energy vs concentration isotherms shown for a range of temperatures.

However, the corresponding concentration profiles for A particles, $x_A(z)$, are linear at small dT/dz and become more and more nonlinear as dT/dz increases [Fig. 6(d)]. This is evident from the spatial profiles of the concentration gradient, dx_A/dz, as shown in Fig. 6(e)—constant for small gradients and otherwise with increasing gradient. We emphasize that these profiles are observed in the steady state and do not reflect any transient behavior. The departure from the linear response is also seen in the dependence of the Soret coefficient (the local slope is calculated over seven bins) with increasing thermal gradient in Fig. 7 (bottom). While it is constant at sufficiently small values of dT/dz, it starts to increase at a gradient of about $dT/dz \approx 5 \times 10^{-3}$. Microscopically, the nonlinear response is associated with a stronger enrichment of the B species at the colder region [cf. the difference in response of density profiles of A and B species with increasing gradient; see Figs. 6(b) and 6(c)].

From the behavior of dx_A/dz, we chart out the transition from linear to nonlinear response for the various T_m in the supercooled liquid in Fig. 8. Here, the important finding is that the linear response regime breaks down at smaller and smaller thermal gradients with decreasing temperature. Such temperature dependence of nonlinearities is reminiscent of the mechanical response of supercooled liquids [33,34], where similar nonlinear effects are observed at increasingly smaller forcing with decreasing ambient temperature.

We note that in the vicinity of $T_{\rm MCT}$, with increasing gradient, local temperatures in the cold region start to fall below $T_{\rm MCT}$. We show one such example in Fig. 9, where for $T_m = 0.5$ and the largest applied gradient the local temperature goes below $T_{\rm MCT} = 0.435$ and consequently steady-state behavior is not obtained within the observed time window.

C. Response at $T_m < T_{\rm VFT}$

Having so far explored the response of supercooled liquids, we now consider the case $T_m = 0.2$ which is below $T_{\rm VFT} \approx 0.3$, i.e., in the glassy regime where relaxation processes are very slow or nearly arrested. If we impose $\Delta T = 0.05$, very soon, a linear temperature profile sets in, and there is a finite heat current between the hot and cold regions; see

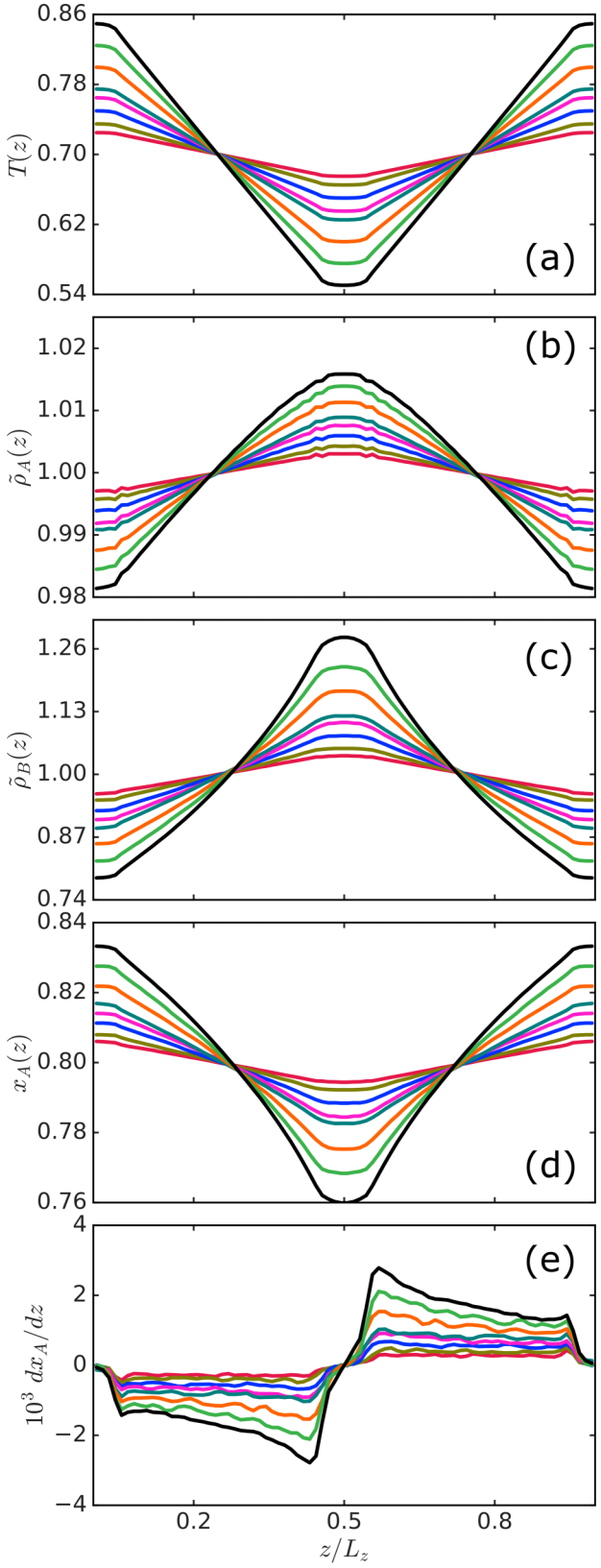

FIG. 6. $T_m = 0.7$: (a) Temperature profiles, $T(z)$, for increasing applied thermal gradient, shown for $(dT/dz)10^3 = 1.33, 1.86, 2.66, 3.45, 3.99, 5.31, 6.64, 7.97$. (b) Corresponding normalized density profiles of A species, and B species (c). (d) Concentration profiles of A particles. (e) Gradient of the concentration profiles shown in (d).

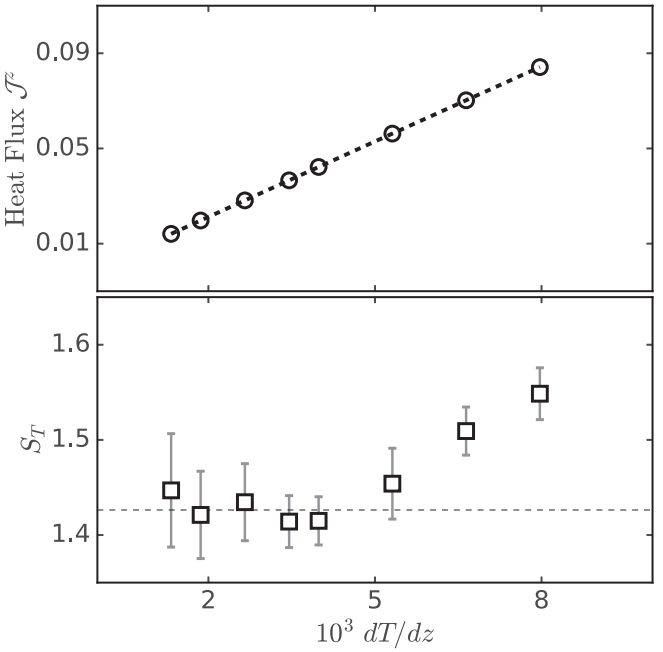

FIG. 7. $T_m = 0.7$. Top: Variation of heat flux J^z with changing imposed temperature gradient (dT/dz): linearity is maintained over the entire range of applied gradients. S_T is computed from the temperature and concentration profiles shown in Figs. 6(a) and 6(d). Bottom: The dashed line corresponds to the average value of S_T in the linear response regime.

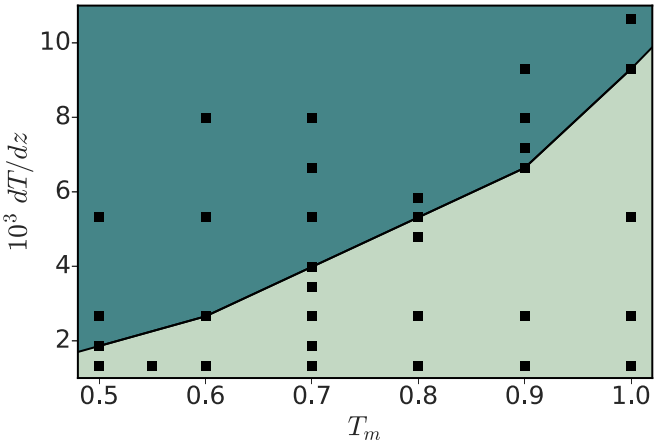

FIG. 8. State diagram in the $\{T_m, dT/dz\}$ plane, indicating where the transition from linear response (light-green area) to nonlinear response (dark-green area) sets in.

Fig. 10 (left). Note that for the applied ΔT all local regions are in the glassy state. Here, unlike the liquid regime, the concentration profile shows no spatial dependence and, for all waiting times after application of the thermal gradient, it is nearly indistinguishable from the one measured for the quiescent aging glass [Fig. 10 (right bottom)]. Thus, for the glass, under applied thermal gradient, the local concentration remains intact, under applied thermal gradient, i.e., the Soret effect is not observed. The density profiles of each species [see Fig. 10 (right top and right middle)] evidence that the majority component, i.e., the A particles, do respond to the thermal gradient, albeit with very small changes in local density due to a local expansion of the volume. In contrast, over the time scale of the observation, the B particles are nearly unresponsive. In other words, the reorganization of the minority species, that is necessary for any concentration variation to happen, as demonstrated earlier, is not induced via the applied thermal gradient, where locally all regions are in the glassy regime.

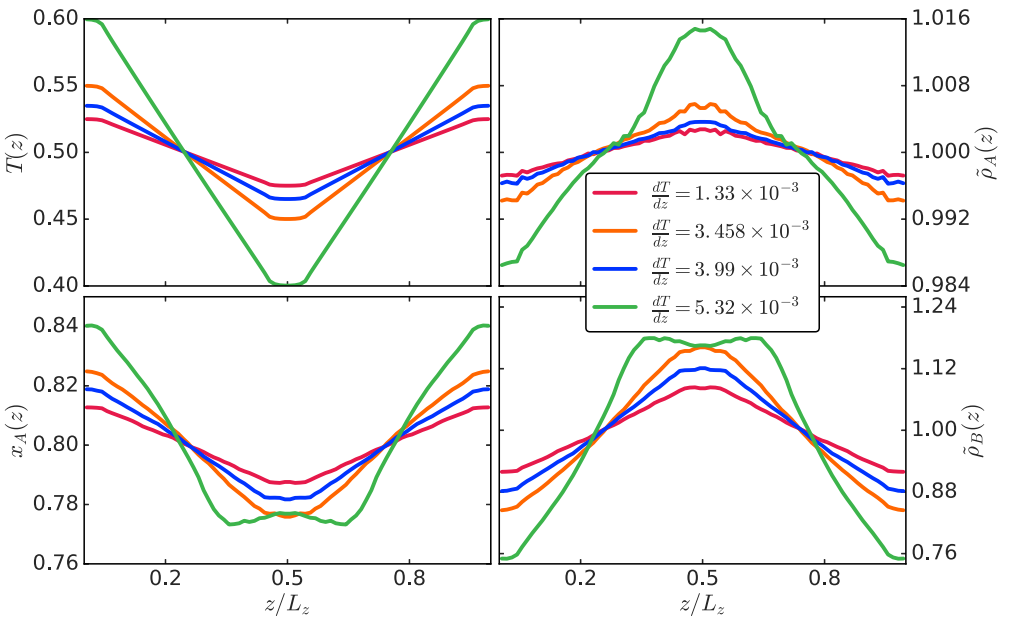

FIG. 9. $T_m = 0.5$. Left: Profiles of temperature (top) and concentration of A particles (bottom), for increasing applied gradient (dT/dz). Right: Corresponding profiles of local density of A (top) and B (bottom) particles, normalized with the respective global density.

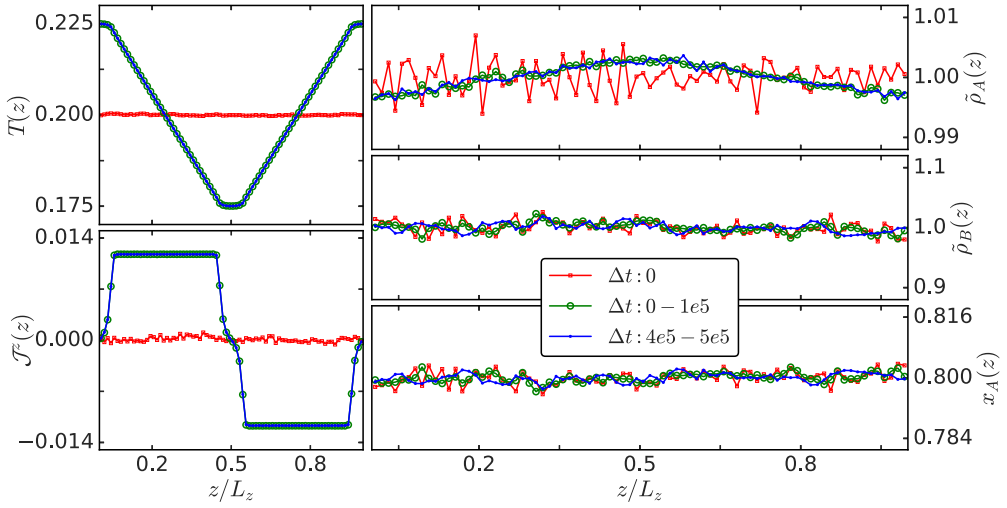

FIG. 10. $T_m = 0.2$, $\Delta T = 0.1$. Left: Spatial profile of applied thermal gradient (top) and corresponding heat current that develops (bottom). Right: Evolution of the spatial profile of normalized density of A species (top), B species (middle), and concentration of A species (bottom), shown for different time windows $\Delta t/10^5 = 0$–1 (blue) and 4–5 (green). Corresponding data for unperturbed system at $T = 0.2$ are shown as dashed lines.

D. Response to a thermal gradient "pulse"

Finally, we consider the following thought experiment for a glass sample, where initially both thermostatted regions are maintained at $T = 0.2$ [regime BG in Fig. 11(a)] and aged under this homogeneous thermal condition for $t_{\text{age}} = 10^4$, after a thermal quench from the high-temperature liquid phase. Under such conditions, there is no spatial variation in x_B, $\tilde{\rho}_B$, $\tilde{\rho}_A$, as should be the case [see Figs. 11(c), 11(f) and 11(i)]. It is, then, suddenly exposed to a thermal gradient [regime DG in Fig. 11(a)], with $T_{\text{h}} = 0.5$ and $T_{\text{c}} = 0.2$, whereby one end of the system is above T_{MCT}, while the other end is much below. Then, the current becomes finite and steady, very soon, and a steady temperature profile is obtained [Fig. 11(b)]. For the A particles, the density profile becomes marginally nonuniform and reaches a steady state [Fig. 11(g)], corresponding to a local thermal expansion, as discussed above. For the B particles, however, the density profile and consequently the concentration profile starts to evolve with time—the local density becomes smaller at the hotter end, as should be the case, and a compaction front slowly propagates towards the cooler end [see Figs. 11(d) and 11(j) for x_B and $\tilde{\rho}_B$, respectively]. Within the window over which the temperature gradient is on ($\Delta t_1 = 5 \times 10^5$), we clearly do not reach a steady state in $\tilde{\rho}_B$ and thus x_B. Then, the gradient is switched off, i.e., both thermostats are again at $T = 0.2$ [regime AG in Fig. 11(a)]. While again the thermal current quickly goes to zero and the marginal density variation in A largely wears off [Fig. 11(h)], after the switch-off, the situation is very

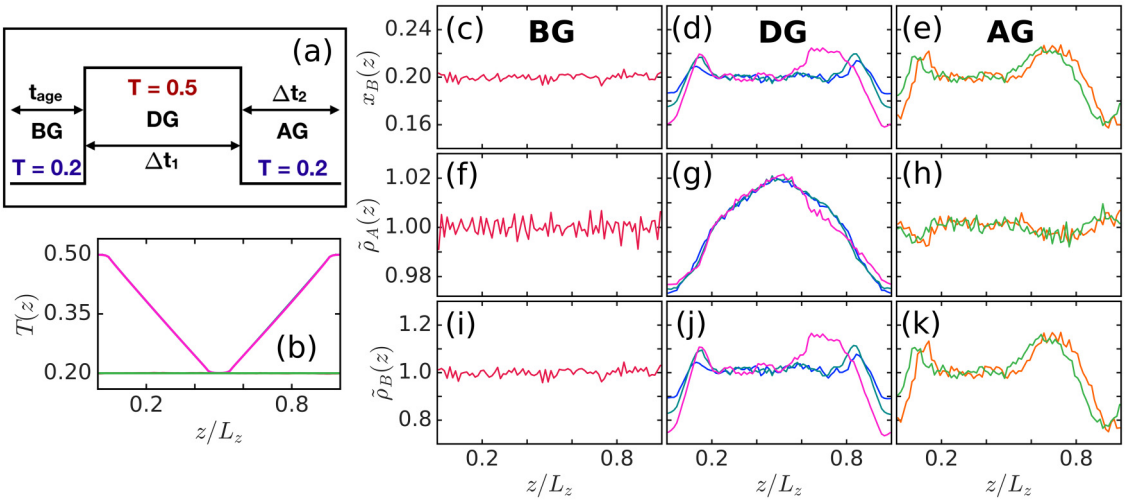

FIG. 11. Response to a thermal gradient *pulse* with $T_{\text{h}} = 0.5$ and $T_{\text{c}} = 0.2$. (a) Schematic of the protocol (see text). (b) Spatial temperature profile during the protocol. Lower panels: Time evolution of the spatial profiles, during BG, DG, and AG (from left to right) for (c)–(e) concentration of B particles, (f)–(h) density of A particles, and (i)–(k) density of B particles. In panels (d), (g), and (j), the curves are shown for $\Delta t/10^4 = 0$–5 (blue), 5–10 (cyan), and 45–50 (magenta). Similarly, in panels (e), (h), and (k), the curves are shown for $\Delta t/10^4 = 4$–5 (orange) and 49–50 (green).

different for the B particles. For them, the density profiles remain almost nonevolving over $\Delta t_2/10^4 = 50$ [Fig. 11(k)], and thereby whatever spatial variation in concentration had occurred with the gradient switched on remains nearly locked in, spatially, under the recovered glassy ambience [Fig. 11(e)].

IV. CONCLUSIONS

We have studied the response of a glass-forming LJ mixture to an applied thermal gradient, in order to explore the interplay of heat transport and interdiffusive processes, as the mean ambient temperature is lowered from the supercooled regime towards the glass transition. Unlike the fast heat transport, structural relaxations and consequently interdiffusion exhibit a drastic slowing down with decreasing temperature. In combination with chemical ordering effects, this results in increased concentration gradients and thereby larger Soret coefficients. Due to the divergence of structural relaxation time scales, such features get suppressed in the glass. Moreover, the linear coupling between heat transport and interdiffusion breaks down when the thermal gradient is large, and the lower bound for this breakdown decreases while approaching the glassy regime. By applying a thermal gradient which leads to local melting of the glass, and then switching it off, we demonstrate that it is possible to freeze in concentration inhomogeneities in a glass. Such a protocol thus provides a possible route to design amorphous solids with specific concentration profiles. More such time-dependent protocols need further exploration to achieve needed functionalities, as well as to understand current practices in different applications, e.g., laser-induced melting or welding. Similarly, controlled experiments using simple glass formers are also necessary to support such computational studies. A recent study using x-ray radiography of an Al-Ni mixture [35] has demonstrated that it is possible to obtain accurate experimental values of the Soret coefficient for real systems with similar properties as the LJ model, considered in this paper. On the theoretical side of understanding such phenomena, limited explorations have occurred from a microscopic perspective, especially in the approach to glass transition, and our paper aims at motivating further studies in this direction.

ACKNOWLEDGMENTS

We thank J.-L. Barrat, C. Dasgupta, F. Bresme, R. Mandal, and P. Bhuyan for useful discussions, and also the high performance computing facilities at the Institute of Mathematical Sciences for providing computing hours.

[1] K. Binder and W. Kob, *Glassy Materials and Disordered Solids: An Introduction to Their Statistical Mechanics, Revised Edition* (World Scientific, Singapore, 2011).
[2] S. R. de Groot and P. Mazur, *Non-Equilibrium Thermodynamics* (Dover, New York, 1984).
[3] C. Ludwig, Sitzungsber. Akad. Wiss. Wien Math.- Naturwiss. Kl. **20**, 539 (1856).
[4] C. Soret, Arch. Sci. Phys. Nat. Genève **3**, 48 (1879).
[5] T. Ikeshoji and B. Hafskjold, Mol. Phys. **81**, 251 (1994).
[6] D. Reith and F. Müller-Plathe, J. Chem. Phys. **112**, 2436 (2000).
[7] P.-A. Artola and B. Rousseau, Phys. Rev. Lett. **98**, 125901 (2007).
[8] J. K. Platten, J. Appl. Mech. **73**, 5 (2006).
[9] W. Köhler and K. I. Morozov, J. Non-Equilib. Thermodyn. **41**, 151 (2016).
[10] J. Armstrong and F. Bresme, Phys. Chem. Chem. Phys. **16**, 12307 (2014).
[11] S. Bonella, M. Ferrario, and G. Ciccotti, Langmuir **33**, 11281 (2017).
[12] C. A. Angell, Solid State Ionics **18**, 72 (1986).
[13] Y. Liu, C. T. Liu, E. P. George, and X. Z. Wang, Appl. Phys. Lett. **89**, 051919 (2006).
[14] D. Clever and J. Lang, Optimal Control Appl. Meth. **33**, 157 (2012).
[15] M. D. Ediger, J. Chem. Phys. **147**, 210901 (2017)
[16] J. Rauch and W. Köhler, Phys. Rev. Lett. **88**, 185901 (2002).
[17] D. Castelvecchi, Physics **5**, 18 (2012).
[18] D. J. Lacks, G. Goel, C. J. Bopp IV, J. A. Van Orman, C. E. Lesher, and C. C. Lundstrom, Phys. Rev. Lett. **108**, 065901 (2012).
[19] Y. Liu, M. Shimizu, B. Zhu, Y. Dai, B. Qian, J. Qiu, Y. Shimotsuma, K. Miura, and K. Hirao, Opt. Lett. **36**, 2161 (2011).
[20] P. J. Bhuyan, R. Mandal, P. Chaudhuri, A. Dhar, and C. Dasgupta, arXiv:1703.04494.
[21] H. Mizuno, S. Mossa, and J.-L. Barrat, Europhys. Lett. **104**, 56001 (2013).
[22] W. Götze and A. Latz, J. Phys.: Condens. Matter **1**, 4169 (1989).
[23] P. Scheidler, W. Kob, A. Latz, J. Horbach, and K. Binder, Phys. Rev. B **63**, 104204 (2001).
[24] W. Kob and H. C. Andersen, Phys. Rev. Lett. **73**, 1376 (1994).
[25] S. Toxvaerd, U. R. Pedersen, T. B. Schroder, and J. C. Dyre, J. Chem. Phys. **130**, 224501 (2009).
[26] U. R. Pedersen, T. B. Schroder, and J. C. Dyre, Phys. Rev. Lett. **120**, 165501 (2018).
[27] S. Amore, J. Horbach, and I. Egry, J. Chem. Phys. **134**, 044515 (2011).
[28] S. Plimpton, J. Comp. Phys. **117**, 1 (1995).
[29] For $T > T_{\mathrm{MCT}}$, profiles are averaged over the two zones between the hot and cold ends, apart from ensemble averaging.
[30] J. Horbach, S. K. Das, A. Griesche, M.-P. Macht, G. Frohberg, and A. Meyer, Phys. Rev. B **75**, 174304 (2007).
[31] A. Baranyai, Phys. Rev. E **54**, 6911 (1996).
[32] C. S. Cargill III and F. Spaepen, J. Non-Cryst. Solids **43**, 91 (1981)
[33] L. Berthier and J.-L. Barrat, J. Chem. Phys. **116**, 6228 (2002).
[34] J. Zausch, J. Horbach, M. Laurati, S. U. Egelhaaf, J. M. Brader, T. Voigtmann, and M. Fuchs, J. Phys.: Condens. Matter **20**, 404210 (2008).
[35] E. Sondermann, F. Kargl, and A. Meyer, Phys. Rev. Lett. **123**, 255902 (2019).